ARMY RESEARCH LABORATORY

Microphysical Influences on Electro-Optic Signal Propagation in Complex Areas

by Arnold Tunick and Gary Carhart

ARL-MR-0633 **December 2005**

NOTICES

Disclaimers

The findings in this report are not to be construed as an official Department of the Army position unless so designated by other authorized documents.

Citation of manufacturer's or trade names does not constitute an official endorsement or approval of the use thereof.

Destroy this report when it is no longer needed. Do not return it to the originator.

Army Research Laboratory
Adelphi, MD 20783-1197

ARL-MR-0633 **December 2005**

Microphysical Influences on Electro-Optic Signal Propagation in Complex Areas

Arnold Tunick and Gary Carhart
Computational and Information Sciences Directorate, ARL

REPORT DOCUMENTATION PAGE

Form Approved
OMB No. 0704-0188

1. REPORT DATE *(DD-MM-YYYY)*	2. REPORT TYPE	3. DATES COVERED (From - To)
December 2005	Final	June to November 2005

4. TITLE AND SUBTITLE
Microphysical Influences on Electro-Optic Signal Propagation in Complex Areas

5a. CONTRACT NUMBER

5b. GRANT NUMBER

5c. PROGRAM ELEMENT NUMBER

6. AUTHOR(S)
Arnold Tunick and Gary Carhart

5d. PROJECT NUMBER

5e. TASK NUMBER

5f. WORK UNIT NUMBER

7. PERFORMING ORGANIZATION NAME(S) AND ADDRESS(ES)
U.S. Army Research Laboratory
ATTN: AMSRD-ARL-CI-CN
2800 Powder Mill Road
Adelphi, MD 20783-1197

8. PERFORMING ORGANIZATION REPORT NUMBER
ARL-MR-0633

9. SPONSORING/MONITORING AGENCY NAME(S) AND ADDRESS(ES)
U.S. Army Research Laboratory
2800 Powder Mill Road
Adelphi, MD 20783-1197

10. SPONSOR/MONITOR'S ACRONYM(S)

11. SPONSOR/MONITOR'S REPORT NUMBER(S)

12. DISTRIBUTION/AVAILABILITY STATEMENT
Approved for public release; distribution unlimited.

13. SUPPLEMENTARY NOTES

14. ABSTRACT

This paper presents a finite-difference computer model to predict the microphysical influences on electro-optic signal propagation in complex areas, e.g., around single and multiple building arrays and forests. The model incorporates physics-based algorithms to account for advection, the pressure gradient, eddy diffusion, and drag forces due to vegetation (e.g., open fields or forests). Note that mechanisms to account for heating, cooling, and moisture flux are not included at this time. Our main concern is to maintain a computationally efficient program code that is also flexible with regard to modifications and debugging. This allows us to apply the computer model to different kinds of tests. Nevertheless, we anticipate that this research will contribute much useful information related to laser optic signal propagation such as the impact of buildings and forests on future optical turbulence (*Cn2*) calculations.

15. SUBJECT TERMS
computational fluid dynamics; wind flow; buildings; forests; optical turbulence; laser optics

16. SECURITY CLASSIFICATION OF:			17. LIMITATION OF ABSTRACT	18. NUMBER OF PAGES	19a. NAME OF RESPONSIBLE PERSON
a. REPORT	b. ABSTRACT	c. THIS PAGE			Arnold Tunick
Unclassified	Unclassified	Unclassified	UL	22	19b. TELEPHONE NUMBER (*Include area code*) 301-394-1765

Standard Form 298 (Rev. 8/98)
Prescribed by ANSI Std. Z39.18

Contents

List of Figures

Acknowledgment

The author gratefully acknowledges Ronald Meyers and Keith Deacon of the U.S. Army Research Laboratory (ARL) for offering helpful comments and discussions on this topic. Partial funding for this study was provided by the U.S. Army Engineer Research and Development Center and ARL.

INTENTIONALLY LEFT BLANK.

1. Introduction

The Army Research Laboratory (ARL), Atmospheric Laser Optics Testbed (A_LOT) is a unique experimental facility with which to measure optical turbulence (*Cn2*) intensity and investigate its effects on infrared imaging and laser optics communications (*1,2*). Within the A_LOT, a near horizontal, 2.3 km optical path extends from the top of a tall water tower to the Intelligent Optics Laboratory (IOL) rooftop at ARL. However, complex microphysical influences, e.g., irregular wind flow patterns around the IOL and the water tower and the effects from wind shears and temperature changes across the top of nearby forest canopies, may affect the A_LOT measured data and research applications. To this end, computer simulation models may provide some meaningful results even though all the pertinent landscape and/or canopy characterization data along the optical path may not yet be known or available.

In a previous study, Tunick (*3*) reported on the characterization of complex (e.g., urban) signal propagation environments via physics-based, computational fluid dynamics (CFD) models. However, CFD program codes are (as a rule) quite computationally intensive (*4,5*). For example, CFD codes can require 1 to 8 hours or more of execution time on multiprocessor super-computers. In addition, CFD models are generally cumbersome to modify and debug. In contrast, it was found that a useful mathematical representation of several key microphysical parameters inside and above forests could be obtained by means of a rapid, steady-state, second-order turbulence closure model, with an embedded radiative transfer and energy budget algorithm to predict the heat source (*6,7*). However, development of this later computer model made it possible to generate realistic profiles for the wind speed and temperature within and above uniform vegetative canopies only. Hence, we desired an intermediary model, which would be computationally efficient and, at the same time, complete in physics to characterize the propagation environment around different building geometries embedded in the model grid (as well representation of canopy drag forces). In other words, we are interested in models that are still reasonably fast but have enough flexibility to apply to the types of field tests envisioned in future works (e.g., studies related to free-space laser optics communications from within the ARL A_LOT).

In this paper, we present a finite-difference computer model to predict the three-dimensional microphysical influences on signal propagation in complex areas, e.g., around single and multiple building arrays and forests. So far, the model accounts for advection, the pressure gradient, and drag forces due to vegetation (e.g., open fields or forests). The model incorporates first-order (eddy diffusivity) turbulence closure for neutral stability (see Mellor and Yamada (*8*)). Note that mechanisms to account for heating, cooling, and moisture flux are not yet considered (in order to maintain computational efficiency and flexibility with regard to modifications and debugging). Nevertheless, our research strategy includes the development of such algorithms,

which can be implemented in future works to improve existing optical turbulence (*Cn2*) modeling and analysis around the ARL A_LOT Facility.

2. Model description

Following the numerical methods discussed by Meyers (*9*) as well as those found in several key texts on fluid mechanics (*10-14*), the simplified Navier Stokes equation (in non-conservative form) for the current model, neglecting Coriolis[1] forces, can be expressed as

$$\frac{\partial \vec{u}}{\partial t} + \vec{u} \cdot \vec{\nabla} \vec{u} = \beta \nabla \left(\vec{\nabla} \cdot \vec{u} \right) + k \nabla^2 \vec{u} + \vec{f} \tag{1}$$

where t is the independent variable time, $\vec{u} = u, v, w$ is the wind velocity vector, β is a constant, k is the eddy viscosity (assumed constant), and $\vec{f}$ is the drag force acceleration due to vegetation. In equation 1, the advection term is

$$\left(\vec{u} \cdot \vec{\nabla} \right) u = \left(u \frac{\partial}{\partial x} + v \frac{\partial}{\partial y} + w \frac{\partial}{\partial z} \right) u , \tag{2a}$$

$$\left(\vec{u} \cdot \vec{\nabla} \right) v = \left(u \frac{\partial}{\partial x} + v \frac{\partial}{\partial y} + w \frac{\partial}{\partial z} \right) v , \tag{2b}$$

and

$$\left(\vec{u} \cdot \vec{\nabla} \right) w = \left(u \frac{\partial}{\partial x} + v \frac{\partial}{\partial y} + w \frac{\partial}{\partial z} \right) w . \tag{2c}$$

The divergence portion of the pressure gradient term is

$$A = \vec{\nabla} \cdot \vec{u} = \frac{\partial u}{\partial x} + \frac{\partial v}{\partial y} + \frac{\partial w}{\partial z} , \tag{3}$$

and the Laplacian portions of the eddy diffusion term are

$$\nabla^2 u = \frac{\partial^2 u}{\partial x^2} + \frac{\partial^2 u}{\partial y^2} + \frac{\partial^2 u}{\partial z^2} , \tag{4a}$$

[1] An earlier survey of the literature (*15*) noted that other than a few authors, e.g., Shinn (*16*), Holland (*17*), and Wilson and Flesch (*18*), most exclude the effect of the Coriolis force as having negligible effect on the scales of motion considered, i.e., wind flow through the forest canopy layer.

$$\nabla^2 v = \frac{\partial^2 v}{\partial x^2} + \frac{\partial^2 v}{\partial y^2} + \frac{\partial^2 v}{\partial z^2}, \tag{4b}$$

and

$$\nabla^2 w = \frac{\partial^2 w}{\partial x^2} + \frac{\partial^2 w}{\partial y^2} + \frac{\partial^2 w}{\partial z^2}. \tag{4c}$$

Finally, the vegetation drag force accelerations are

$$f_x = C_d A|\vec{u}|u, \tag{5a}$$

$$f_y = C_d A|\vec{u}|v, \tag{5b}$$

and

$$f_z = C_d A|\vec{u}|w, \tag{5c}$$

where C_d is the drag coefficient (0.1-0.2), A is the leaf area density (see ref. (*6*)), and $|\vec{u}|$ is the magnitude of the total wind.

Equation 1 is solved explicitly forward in time, with the advection term upwind differenced in space and the diffusion term central differenced in space. As an example, the equation for the *u*-component of the wind can be discretized as

$$u_{i,j,k}^{n+1} = u_{i,j,k}^{n} + \Delta t \left[\begin{array}{l} -\left(u_{i,j,k}^{n}\left(\frac{u_{i,j,k}^{n} - u_{i-1,j,k}^{n}}{\Delta x} \right) + v_{i,j,k}^{n}\left(\frac{u_{i,j,k}^{n} - u_{i,j-1,k}^{n}}{\Delta y} \right) + w_{i,j,k}^{n}\left(\frac{u_{i,j,k}^{n} - u_{i,j,k-1}^{n}}{\Delta z} \right) \right) \\ + \beta\left(\frac{A_{i+1,j,k}^{n} - A_{i-1,j,k}^{n}}{2\Delta x} \right) \\ + k\left(\frac{u_{i+1,j,k}^{n} - 2u_{i,j,k}^{n} + u_{i-1,j,k}^{n}}{(\Delta x)^2} + \frac{u_{i,j+1,k}^{n} - 2u_{i,j,k}^{n} + u_{i,j-1,k}^{n}}{(\Delta y)^2} + \frac{u_{i,j,k+1}^{n} - 2u_{i,j,k}^{n} + u_{i,j,k-1}^{n}}{(\Delta z)^2} \right) \\ + C_d A\left[\left(u_{i,j,k}^{n}\right)^2 + \left(v_{i,j,k}^{n}\right)^2 + \left(w_{i,j,k}^{n}\right)^2 \right]^{1/2} \cdot u_{i,j,k}^{n} \end{array} \right]. \tag{6}$$

The boundary conditions applied in this model are as follows: inflow (typically from the west) is a specified value (Dirichlet boundary condition), such as a constant or log-law velocity profile. Outflow (typically to the east) is constrained to have a constant flux, i.e., zero gradients (Neumann boundary condition). The north and south sides are also constrained to have a constant flux. The vertical velocity at the bottom of the model is a specified value (e.g., $w = 0$) and at the model top the vertical velocity has a zero gradient.

3. Model results

The model was applied to four cases, i.e., a single building in the center of the grid to test wind flow symmetry, an array of five buildings (also to simulate wind flow symmetry), a forest canopy centered in the model grid to simulate leading edge flow separation, and a larger and more complex building array to simulate wind flow characteristics around the IOL and adjacent ARL structures. Grid spacing for the single and multiple building array was uniform, i.e., $\Delta x = \Delta y = \Delta z = 1.0$ m, where the number of grid points was 27 x 27 x 12 for the single building and 50 x 50 x 20 for the array. Here, $\Delta t = 0.001$ *s* and the model was executed for 14K time-steps. For the forest application, the grid spacing was $\Delta x = \Delta y = 2.0$ *m* and $\Delta z = 1.0$ *m*, where the number of grid points was 60 x 60 x 30. Here, $\Delta t = 0.001$ *s* and the model was executed for 40K time-steps. For the IOL and adjacent buildings, the grid spacing was $\Delta x = \Delta y = 2.5$ *m* and $\Delta z = 2.0$ *m*, where the number of grid points was 100 x 100 x 25. Here, in contrast, $\Delta t = 0.001$ *s* and the model was executed for 20K time-steps. The computer model was executed on a 1.8 GHz desktop PC with approximately 512 MB RAM. Model runtimes were approximately 2 minutes for the single building, 20 minutes for the five building array, 50 minutes for the forest canopy, and 2 hours and 20 minutes for the IOL and adjacent buildings.

Figure 1 presents horizontal and vertical cross-sections of the vector wind field around a single building located in the middle of the model grid. Here, the initial wind velocities are $u = 3.0\ ms^{-1}$ and $v = w = 0.0\ ms^{-1}$. The horizontal cross-section is taken at $z = 5.0$ *m* above ground level. This result is very encouraging. The wind flow patterns going around (and over the top of) the single building appear quite reasonable.

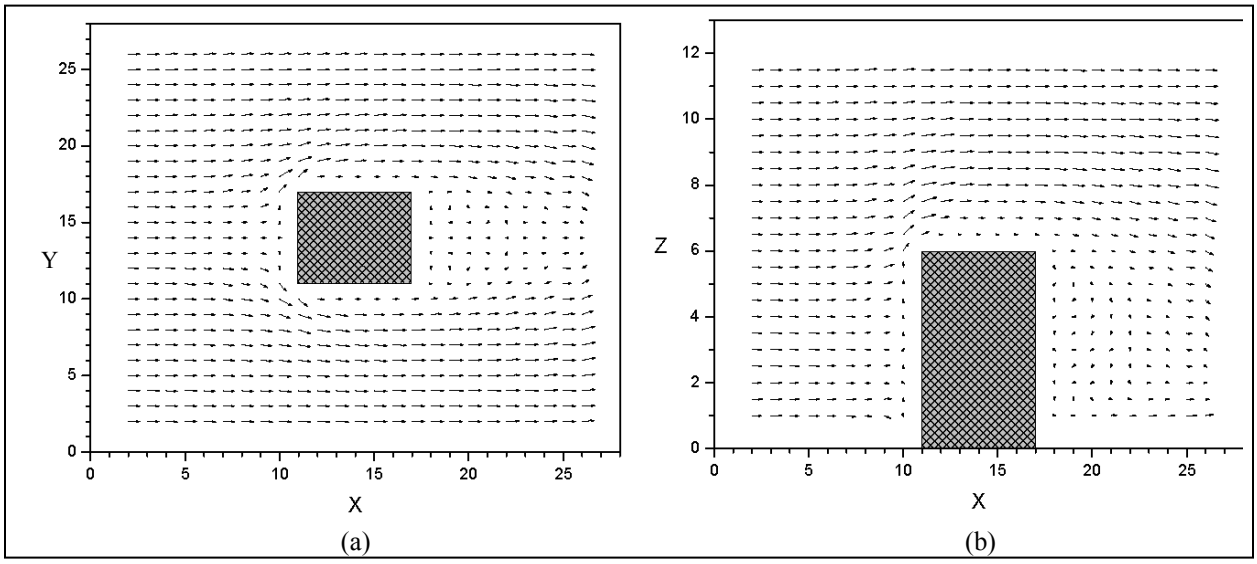

Figure 1. Horizontal (a) and vertical (b) cross-section of the vector wind field around a single building. Initial wind velocities are $u = 3.0\ ms^{-1}$ and $v = w = 0.0\ ms^{-1}$. The horizontal cross-section is taken at $z = 5.0$ *m*.

Figure 2 presents horizontal and vertical cross-sections of the vector wind field around a five building array. Again, the initial wind velocities are $u = 3.0\ ms^{-1}$ and $v = w = 0.0\ ms^{-1}$ and the cross-sections are taken at $y = 13.0\ m$ from the south edge and $z = 5.0\ m$ above ground level. These results are also quite encouraging, especially since they provide good visual confirmation (i.e., strong symmetry) that the program coding is error-free.

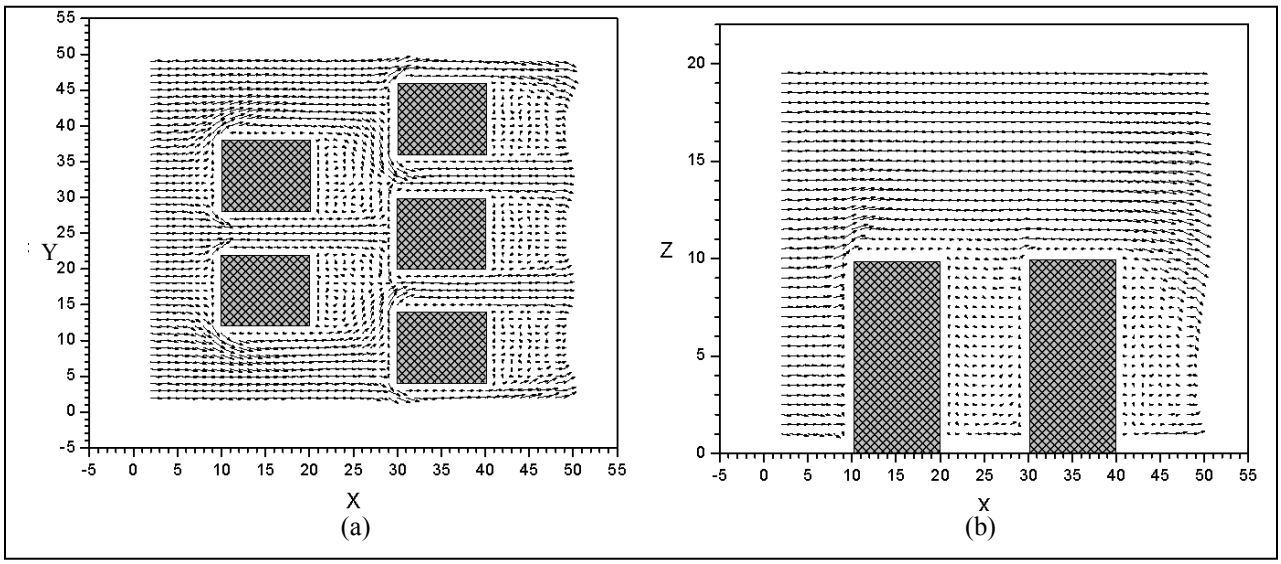

Figure 2. Horizontal (a) and vertical (b) cross-section of the vector wind field around a five building array. The initial wind velocities are $u = 3.0\ ms^{-1}$ and $v = w = 0.0\ ms^{-1}$. The horizontal cross-section is taken at $y = 13.0\ m$ and $z = 5.0\ m$.

Figure 3 presents vertical cross-sections of the wind field around a uniform forest canopy located in the middle of the model grid. The canopy height is $h = 15.0\ m$. The leaf area index is LAI = 4. In addition, a generic leaf area density profile is assumed (see ref. *6,7*). Although somewhat difficult to visualize using small vector arrows, the wind field (shown in figure 3a) does separate (diverge) at the forest edge. Part of the flow goes downward into the trunk space of the forest, below the layer of leaves and branches, and part of the flow goes upward through the canopy top and above. While streamlines may be generated in future works to better visualize these model data, this result is highly consistent with previously published works (*16, 19, and 20*). Moreover, figure 3b shows clearly that the magnitude of the winds decrease with distance into the forest (due to cumulative drag effects), especially in the upper half of the forest stand. In addition, secondary, low level wind speed maxima develop through the forest leading edge.

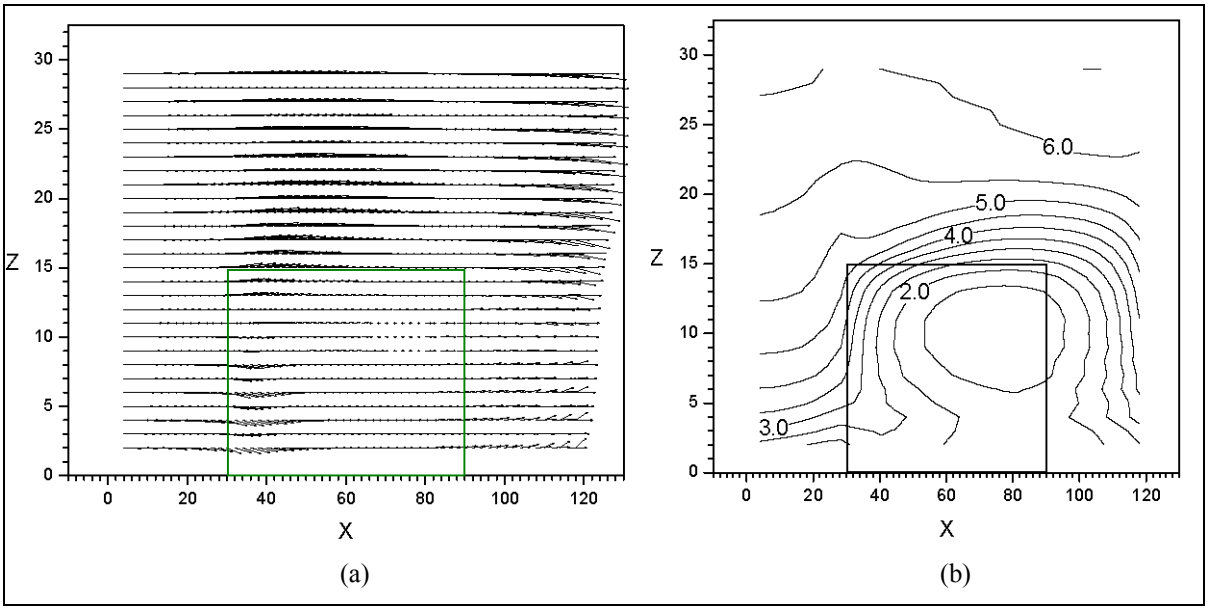

Figure 3. Vertical cross-section of (a) the vector wind field and (b) wind velocity contours (units ms^{-1}) around a uniform forest canopy. The canopy height is $h = 15.0\ m$. The leaf area index is LAI = 4.

Figure 4 presents selected wind velocity profiles taken from the model data shown in figure 3, i.e., the initial wind velocity (log-law) profile, the profile +20 m upwind, the profile at the leading edge, the profile at the forest center, the profile at the trailing edge, and the profile +20 m downwind of the forest. The wind speed profile in the open fields is logarithmically increasing with height above the roughness plane. Inside the forest, the winds are shown to decrease rapidly as momentum becomes depleted through the layers of leaves and branches (due to increased drag). In addition, for the profile in the forest center, the model produces a secondary wind speed maximum at a height of about $z = 4.0\ m$. Shinn (*16*) and Shaw (*21*) discuss such low-level wind maxima in detail. Note that the model results shown here will be sensitive to variations in the assumed leaf area index (LAI) and leaf area density distribution in the canopy (*6,7*).

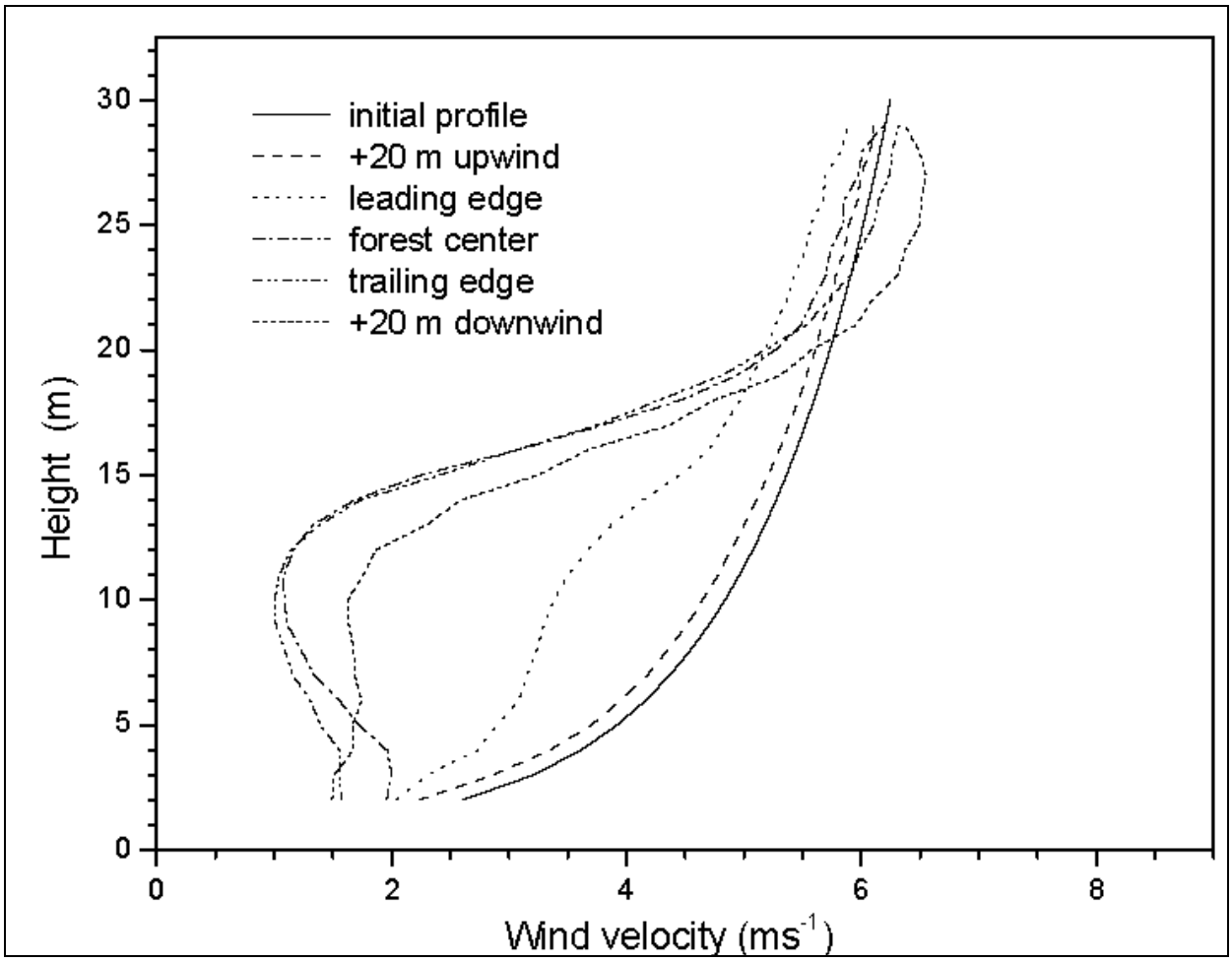

Figure 4. Selected wind velocity profiles taken from the results shown in figure 3, i.e., the initial wind velocity (log-law) profile (solid line), the profile +20 m upwind (large dashed line), at the leading edge (dotted line), at the forest center (dash-dotted line), at the trailing edge (dash-double dotted line), and +20 m downwind of the forest (small dashed line).

Figure 5 presents a horizontal cross-section of the vector wind field around the IOL and adjacent buildings. Here, the initial wind velocities are $u = w = 0.0\ ms^{-1}$ and $v = 4.0\ ms^{-1}$. The horizontal cross-section is taken at $z = 6.0\ m$ above ground level. The (dashed) outlined area identifies forests along the western border of the building complex, for which a constant drag force with height (up to the canopy top, $h = 18.0\ m$) is assumed. More complete canopy characterization data, like those implemented in the previous example, may be incorporated in future works. Nevertheless, this model result is very appealing. It demonstrates that we have completed several successful steps towards obtaining a useful mathematical representation of the wind flow around the IOL and adjacent buildings. Naturally, these results (as well as those shown above) will need to be confirmed by measurements. Yet, if determined to be realistic, this kind of data will be very important for electro-optic and acoustic characterization and prediction.

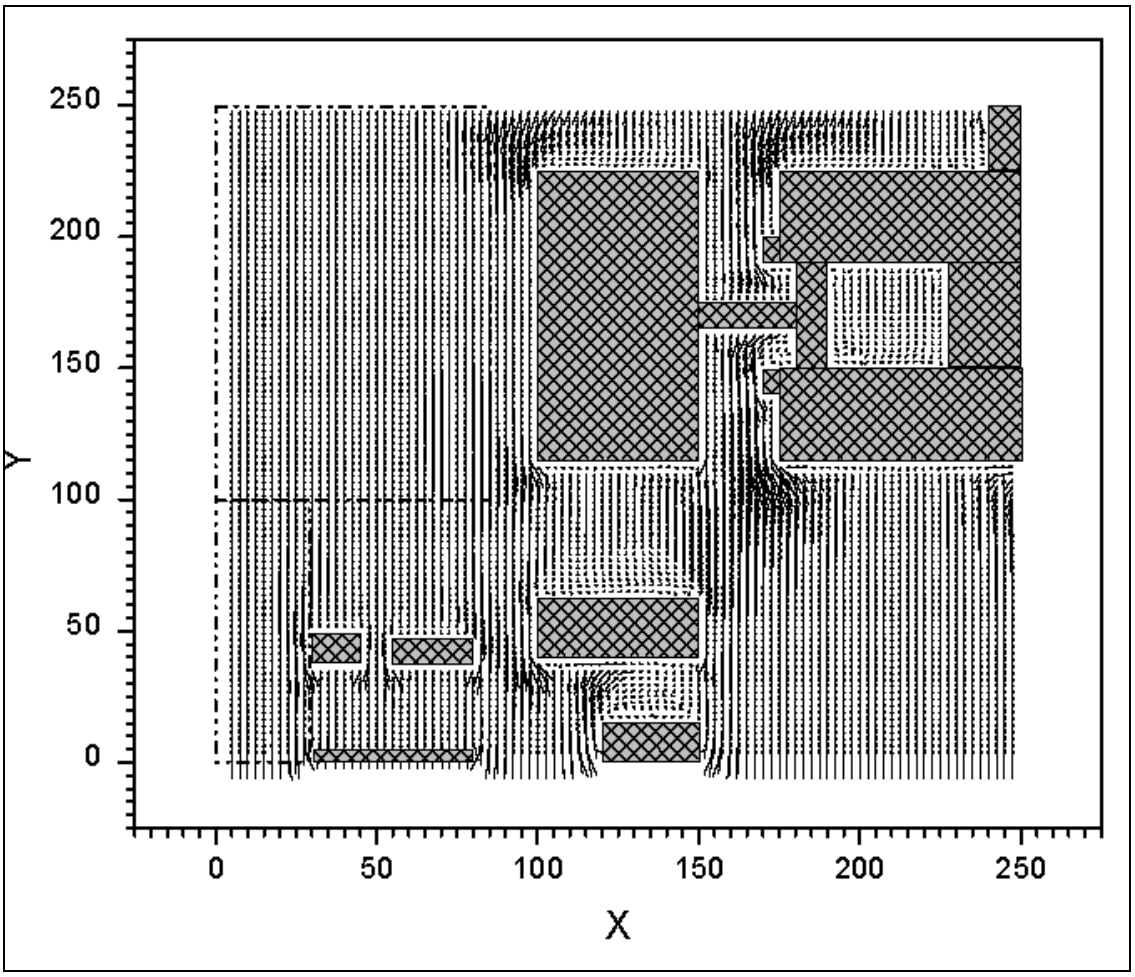

Figure 5. Horizontal cross-section of the vector wind field around the IOL and adjacent buildings. The initial wind velocities are $u = w = 0.0\ ms^{-1}$ and $v = 4.0\ ms^{-1}$. The horizontal cross-section is taken at $z = 6.0\ m$ above ground level. The outlined (dashed-double dotted) area identifies forests along the western border of the building complex.

4. Discussion

Note that the wind flow model presented in this report is still a program code in development, even though it already exhibits some powerful capabilities. Additional algorithms and/or alternate numerical schemes may be implemented in future works to improve the model. For example, temperature and moisture prediction may be investigated via the following expressions, i.e.,

$$\frac{\partial \theta}{\partial t} = -\left(\frac{\partial u\theta}{\partial x} + \frac{\partial v\theta}{\partial y} + \frac{\partial w\theta}{\partial z} \right) + \kappa_\theta \left(\frac{\partial^2 \theta}{\partial x^2} + \frac{\partial^2 \theta}{\partial y^2} + \frac{\partial^2 \theta}{\partial z^2} \right) + S_\theta , \tag{7}$$

and

$$\frac{\partial q}{\partial t} = -\left(\frac{\partial uq}{\partial x} + \frac{\partial vq}{\partial y} + \frac{\partial wq}{\partial z} \right) + \kappa_q \left(\frac{\partial^2 q}{\partial x^2} + \frac{\partial^2 q}{\partial y^2} + \frac{\partial^2 q}{\partial z^2} \right) + S_q , \tag{8}$$

where θ is air temperature (in units ºK), q is specific humidity (in units kg kg^{-1}), κ_θ and κ_q are the eddy diffusivities for heat and water vapor, respectively (in units m^{2}s^{-1}), and S_θ and S_q are the source terms for heat and moisture. The quantity S_θ for forests can be determined via the radiation and energy budget equations presented in (*7*). Alternately, a simpler form for the heat source was shown by Shaw and Schumann (*22*), i.e.,

$$S_\theta = \frac{dQ(z)}{dz}, \tag{9}$$

where $Q(z) = Q(h)\exp(-\alpha F)$. Here, Q is the kinematic heat flux, h is the height of the canopy top, $\alpha = 0.6$ is an extinction coefficient, and $F = \int_z^h A dz$ is the non-dimensional cumulative leaf area index. Naturally, for open fields, buildings, and/or pavement, other suitable heat source, moisture source, and energy budget relations can be applied.

Overall, we expect that the current research (when completed) will be quite useful to improve optical turbulence intensity (*Cn2*) prediction and analysis around the ARL A_LOT Facility. Our work will also contribute towards improved estimates of other key signal propagation parameters, such as the variance in angle-of-arrival fluctuation and the log-intensity variance of transmitted electromagnetic signals. As an example, for propagation across distances less than or equal to approximately 4 km, Beland (*23*) gives an expression for the variance in angle-of-arrival fluctuation for spherical waves as,

$$\left\langle \sigma_A^2 \right\rangle = \; 2.914 \; D^{-\frac{1}{3}} \int_0^L C_n^2(z) \left(\frac{z}{L} \right)^{\frac{5}{3}} dz , \tag{10}$$

for $D >> (\lambda L)^{\frac{1}{2}}$, where D (≈ 0.090 m, possibly) is aperture diameter, λ (≈ 0.94 μm, possibly) is wavelength, L is optical path length, and z is the vertical coordinate. Analogous expressions have been presented for the log-intensity (or log-amplitude) variance of transmitted electromagnetic signals, so that the measure of the path-averaged *Cn*2 due to scintillation (i.e., temporal fluctuations) for a spherical wave can be expressed as,

$$\left\langle \sigma_x^2 \right\rangle = \; 0.56 \; k^{\frac{7}{6}} \int_0^L C_n^2(z) \left(\frac{z}{L} \right)^{\frac{5}{6}} (L - z)^{\frac{5}{6}} \, dz \tag{11}$$

where k is the wave propagation constant $\left(2\pi / \lambda \right)$. Thus, if improved microphysical characterization models will provide better estimates of *Cn*2 along more complex optical lines-

of-site, then better estimates of beam displacement, $\left\langle \sigma_A^2 \right\rangle$, and intensity fluctuations, $\left\langle \sigma_x^2 \right\rangle$, are the kinds improved work product that may be useful in sensor performance (and/or sensor data) analysis. Note that for model evaluation purposes, the ARL A_LOT can provide time series of optical turbulence (scintillometer) and other pertinent data, e.g., like those shown in figure 6.

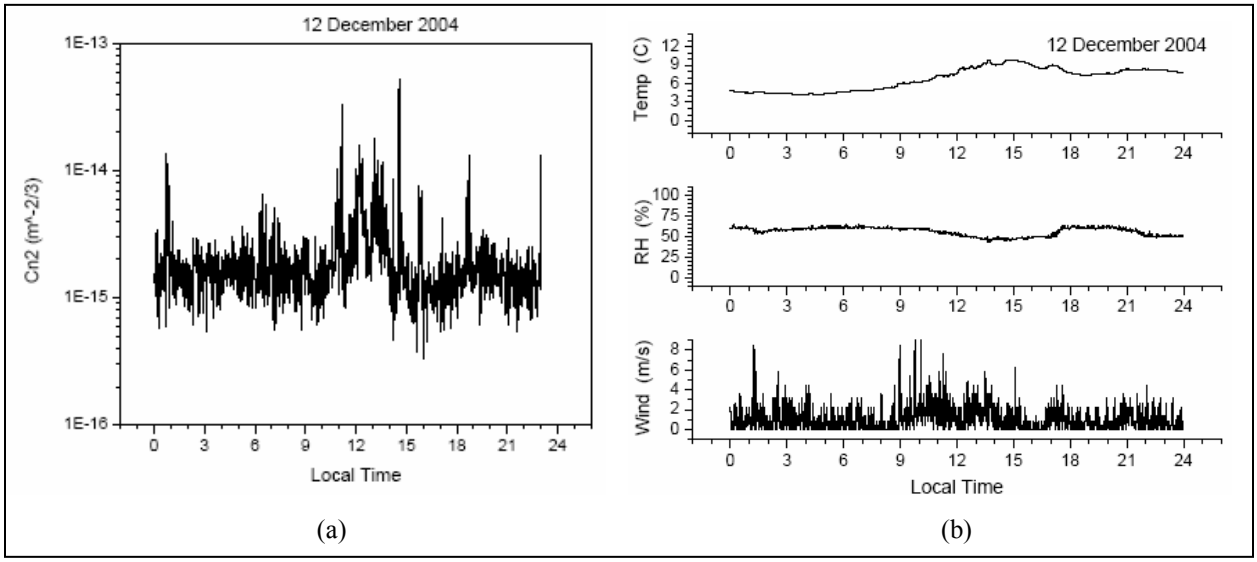

Figure 6. Time series of (a) path-averaged optical turbulence (scintillometer) data and (b) microphysical characterization data collected at the ARL A_LOT Facility on 12 December 2004.

Finally, a useful expression for the refractive index structure parameter (*24-26*) is,

$$C_n^2(z) = b\frac{K_h}{\varepsilon^{1/3}}\left(\frac{\partial n}{\partial z}\right)^2, \tag{12}$$

where b is a constant, K_h is the turbulent exchange coefficient for heat, ε is the energy dissipation rate, and $\partial n/\partial z$ is the vertical gradient of the index of refraction (n). In equation 12, the vertical gradient of the index of refraction for visible and near-infrared wavelengths (0.36 to 3 μm) can be expressed as a function of the partial derivatives for potential temperature ($\partial\theta/\partial z$) and moisture (specific humidity) ($\partial q/\partial z$), i.e.,

$$\frac{\partial n_v}{\partial z} = \left(-M_1(\lambda)\frac{P}{T^2} - 1.61(M_2(\lambda) - M_1(\lambda))\frac{Pq}{T^2}\right)x\,10^{-6}\frac{\partial\theta}{\partial z} + 1.61(M_2(\lambda) - M_1(\lambda))\frac{P}{T}x\,10^{-6}\frac{\partial q}{\partial z} \tag{13}$$

where the dispersion formulas (as functions of wavelength^{-1}, i.e., $\sigma = \lambda^{-1}$) are,

$$M_1(\lambda) = 23.7134 + \frac{6839.397}{130 - \sigma^2} + \frac{45.473}{38.9 - \sigma^2}, \tag{14}$$

and

$$M_2(\lambda) = 64.8731 + 0.58058\,\sigma^2 - 0.007115\,\sigma^4 + 0.0008851\,\sigma^6 . \tag{15}$$

5. Summary and Conclusions

This report presented a new finite-difference computer model to predict the surface layer wind flow around single and multiple building arrays and forest canopies. The model accounts for advection, the pressure gradient, diffusion, and drag forces due to vegetation. The model code is computationally efficient and extremely flexible with regard to modifications and debugging. Our initial model results are quite encouraging. Hence, we have successfully demonstrated new capabilities towards obtaining a useful mathematical representation of microphysical characterization data around the IOL and adjacent buildings. In conclusion, we expect that these kinds of simulation codes will be an important vehicle for investigating optical turbulence intensity (*Cn2*) and related laser-optics propagation effects in and around complex environments.

References

1. Vorontsov M.; Carhart, G.; Banta, M.; Weyrauch, T.; Gowens, J.; Carrano, J. Atmospheric Laser Optics Testbed (A_LOT): Atmospheric propagation characterization, beam control, and imaging results. *In Proc. SPIE Vol. 5162 Advanced Wavefront Control: Methods, Devices, and Applications*, J. D. Gonglewski, M. A. Vorontsov, and M. T. Gruneisen (Eds.), SPIE, Bellingham, WA, 2003.

2. Tunick, A.; Tikhonov, N.; Vorontsov, M.; Carhart, G. *Characterization of optical turbulence (Cn2) data measured at the ARL A_LOT facility*; ARL-MR-625; U.S. Army Research Laboratory: Adelphi, MD, September 2005.

3. Tunick A. *Critical assessment of selected urban microclimate model frameworks*. ARL-MR-619; U.S. Army Research Laboratory: Adelphi, MD, June 2005.

4. Blocken, B.; Carmeliet, J. Pedestrian wind environment around buildings: Literature review and practical examples. *Journal of Thermal Environment & Building Science* **2004**, *28*, 107-159.

5. Vardoulakis, S.; Fisher, B.E.A.; Pericleous, K.; Gonzolez-Flesca, N. Modelling air quality in street canyons: a review. *Atmospheric Environment* **2003**, *37*, 155-182.

6. Tunick A. Calculating the micrometeorological influences on the speed of sound through the atmosphere in forests. *Journal of the Acoustical Society of America* **2003**, *114*, 1796-1806.

7. Tunick, A. A radiation and energy budget algorithm for forest canopies. *Meteorology and Atmospheric Physics* **2006**, *91*, 237-246.

8. Mellor, G. L.; Yamada, T. A hierarchy of turbulence closure models for planetary boundary layer. *Journal of the Atmospheric Sciences* **1974**, *31*, 1791-1806.

9. Meyers, R. E. Personal communication, 2005.

10. Monin, A. S.; Yaglom, A. M. *Statistical Fluid Mechanics*; MIT Press: Cambridge, MA, 769 1971.

11. Hinze, J. O. *Turbulence*; McGraw-Hill: New York, 800, 1975.

12. Schlichting, H. *Boundary Layer Theory*; McGraw-Hill: New York, 817, 1979.

13. Zak, M.; Zbilut, J. P.; Meyers, R. E. *From Instability to Intelligence: Complexity and Predictability in Nonlinear Dynamics*; Springer-Verlag: Lecture Notes in Physics, 552, 1997.

14. Ferziger, J. H.; Perić, M. *Computational Methods for Fluid Dynamics*; 3rd Edition, Springer, Berlin, 423, 2002.

15. Tunick, A. *Coupling Meteorology to Acoustics in Forests*; ARL-MR-538; U.S. Army Research Laboratory: Adelphi, MD, September 2002.

16. Shinn, J. H. *Steady-state two-dimensional air flow in forests and the disturbance of surface layer flow by a forest wall*; ECOM-5383; U.S. Army Electronics Command: Fort Monmouth, NJ, 1971.

17. Holland, J. Z. On pressure-driven wind in deep forests. *Journal of Applied Meteorology* **1989**, *28*, 1349-1355.

18. Wilson, J. D.; Flesch, T. K. Wind and remnant tree sway in forest cutblocks. III. A wind flow model to diagnose spatial variation. *Agricultural and Forest Meteorology* **1999**, *93*, 259-282.

19. Li, Z.; Lin, J. D.; Miller, D. R. Air flow over and through a forest edge: A steady-state numerical simulation. *Boundary-Layer Meteorology* **1990**, *51*, 179-197.

20. Tunick, A. *A two-dimensional meteorological computer model for the forest canopy*; ARL-MR-569; U.S. Army Research Laboratory: Adelphi, MD, 2003.

21. Shaw, R. H. Secondary wind speed maxima inside plant canopies. *Journal of Applied Meteorology* **1977**, *16*, 514-521.

22. Shaw, R. H.; Schumann, U. Large-eddy simulation of turbulent flow above and within a forest. *Boundary Layer Meteorology* **1992**, *61*, 47–64.

23. Beland, R. R. Propagation through atmospheric turbulence. *In The Infrared Electro-Optical Systems Handbook*, J. S. Accetta and D. L. Shumaker (Eds.), SPIE Press Monograph, PM10, Bellingham, WA, 1993.

24. Andreas, E. L. Estimating *Cn*2 over snow and sea ice from meteorological data. *Journal of the Optical Society of America* **1988**, *5*, 481-495.

25. Tatarski, V. I. *The Effects of the Turbulent Atmosphere on Wave Propagation*. Israel Program for Scientific Translations, Jerusalem, 472, 1971.

26. Wesely, M. L. The combined effect of temperature and humidity fluctuations on refractive index. *Journal of Applied Meteorology* **1976**, *15*, 43-49.

Distribution List

ADMNSTR
DEFNS TECHL INFO CTR
ATTN DTIC-OCP (ELECTRONIC COPY)
8725 JOHN J KINGMAN RD STE 0944
FT BELVOIR VA 22060-6218

DARPA
ATTN IXO S WELBY
3701 N FAIRFAX DR
ARLINGTON VA 22203-1714

SCI & TECHNLGY CORP
10 BASIL SAWYER DR
HAMPTON VA 23666-1293

US ARMY CRREL
ATTN CERCL-SI E L ANDREAS
72 LYME RD
HANOVER NJ 03755-1290

NAV POSTGRADUATE SCHL
DEPT OF METEOROLOGY
ATTN P FREDERICKSON
1 UNIVERSITY CIR
MONTEREY CA 93943-5001

AIR FORCE
ATTN WEATHER TECHL LIB
151 PATTON AVE RM 120
ASHEVILLE NC 28801-5002

COLORADO STATE UNIV
DEPT OF ATMOS SCI
ATTN R A PIELKE
200 WEST LAKE STREET
FT COLLINS CO 80523-1371

THE CITY COLLEGE OF NEW YORK
DEPT OF EARTH & ATMOS SCI
ATTN S D GEDZELMAN
J106 MARSHAK BLDG 137TH AND
CONVENT AVE
NEW YORK CITY NY 10031

UNIV OF ALABAMA AT HUNTSVILLE
DEPT OF ATMOS SCI
ATTN R T MCNIDER
HUNTSVILLE AL 35899

NATL CTR FOR ATMOS RSRCH
ATTN NCAR LIBRARY SERIALS
PO BOX 3000
BOULDER CO 80307-3000

US ARMY RSRCH LAB
ATTN AMSRD-ARL-CI-OK-TP
TECHL LIB T LANDFRIED (2 COPIES)
ABERDEEN PROVING GROUND MD 21005-
5066

DIRECTOR
US ARMY RSRCH LAB
ATTN AMSRD-ARL-RO-EN
W D BACH
PO BOX 12211
RESEARCH TRIANGLE PARK NC 27709

US ARMY RSRCH LAB
ATTN AMSRD-ARL-D J M MILLER
ATTN AMSRD-ARL-CI J W GOWENS
ATTN AMSRD-ARL-CI-C
L TOKARCIK
ATTN AMSRD-ARL-CI-C
W F INGRAM
ATTN AMSRD-ARL-CI-C
M VORONTSOV
ATTN AMSRD-ARL-CI-CN
A TUNICK (15 COPIES)
ATTN AMSRD-ARL-CI-CN
G CARHART
ATTN AMSRD-ARL-CI-CN G RACINE
ATTN AMSRD-ARL-CI-CS R MEYERS
ATTN AMSRD-ARL-CI-CS K DEACON
ATTN AMSRD-ARL-CI-OK-T
TECHL PUB (2 COPIES)
ATTN AMSRD-ARL-CI-OK-TL
TECHL LIB (2 COPIES)
ATTN AMSRD-ARL-D J ROCCHIO
ATTN IMNE-ALC-IMS
MAIL & RECORDS MGMT
ADELPHI, MD 20783-1197